crystals

MDPI

Article

Physicochemical, Photocatalytic, Antibacterial, and Antioxidant Screening of Bergenia Ciliata Mediated Nickel Oxide Nanoparticles

Fazal Ur Rehman [1], Rashid Mahmood [1], Manel Ben Ali [2], Amor Hedfi [2], Amine Mezni [3], Sirajul Haq [1,*], Salah Ud Din [1] and Rimsha Ehsan [1]

[1] Department of Chemistry, University of Azad Jammu and Kashmir, Muzffarabad 13100, Pakistan; fazal.rehman@ajku.edu.pk (F.U.R.); rashid.mehmood@ajku.edu.pk (R.M.); salah.mahsud@ajku.edu.pk (S.U.D.); rimsha.ehsan.mphil@ajku.edu.pk (R.E.)
[2] Department of Biology, College of Sciences, Taif University, P.O. Box 11099, Taif 21944, Saudi Arabia; mjbinali@tu.edu.sa (M.B.A.); o.zaied@tu.edu.sa (A.H.)
[3] Department of Chemistry, College of Science, Taif University, P.O. Box 11099, Taif 21944, Saudi Arabia; a.rachid@tu.edu.sa
* Correspondence: siraj.ulhaq@ajku.edu.pk

Abstract: This study was planned to synthesize a multifunctional nanomaterial that can effectively encounter the organic pollutants, multidrug-resistant bacteria and reactive free radicals. The *Bergenia ciliate (B. ciliate)* leaves extract was used as a reducing and capping agent for the synthesis of nickel oxide nanoparticles (NiO NP). The physicochemical properties were studied through X-ray diffractometre (XRD), energy dispersive X-ray (EDX), scanning electron microscopy (SEM), transmission electron microscopy (TEM), UV-visible and Fourier transform infrared (FTIR) spectroscopies. The highly crystalline monoclinic NiO NPs were synthesized with crystallite size of 27.45 nm. The average particle size derived from TEM micrograph was 49.35 nm whereas the calculated band gap for NiO NPs was 3.78 eV. The photocatalytic study shows that 92.17% of the rhodamine 6G (Rh-6G) was efficiently degraded in the presence of NiO NPs. The agar well diffusion method was applied to examine the antibacterial activity of NiO NPs and the activity was found higher against Gram-negative bacteria (GNB) as compared to Gram-positive bacteria (GPB). The ABTS free radical scavenging activity was also performed, however, the activity was found less than the standard.

Keywords: green synthesis; nickel oxide; microscopy; monoclinic; polyhedral

Citation: Rehman, F.U.; Mahmood, R.; Ali, M.B.; Hedfi, A.; Mezni, A.; Haq, S.; Din, S.U.; Ehsan, R. Physicochemical, Photocatalytic, Antibacterial, and Antioxidant Screening of Bergenia Ciliata Mediated Nickel Oxide Nanoparticles. *Crystals* **2021**, *11*, 1137. https://doi.org/10.3390/cryst11091137

Academic Editor: Marilena Carbone

Received: 8 August 2021
Accepted: 15 September 2021
Published: 18 September 2021

1. Introduction

The breakneck engineering achievements and the urbanization with increasing population growth have provoked the massive extrication of the toxic contaminants in the air and water, thus polluting these precious resources. Amongst all the sources of these contaminants, the most distinct are the azo dyes that are hazardous and non-biodegradable produced by the commercial manufacturers [1]. Damping of these dyes in the water and surroundings by the industries is lethal to human health and safety and is a cause of environmental contamination. Moreover, these dyes are damaging the aquatic environment by affecting the watery plants and interrupting the photosynthesis in aquatic flora. In view of all these consequences there is an urgent need to convert these hazardous materials to non-hazardous materials [1,2]. Various methods employed for the treatment of these toxic substances include coagulation, active sludge, reverse osmosis and electrochemical oxidation, but the organic compounds seemed to be stable against chemicals and the treatments and were still persistent in the water even after these treatments [3]. Recently, photocatalytic degradation has been suggested as an environment friendly and inexpensive method to eradicate the organic materials and pollutants from the waste water on manipulating the semiconductor metal oxides like TiO_2, ZnO, CuO and NiO [4].

Moreover the introduction of various herbicides, fungicides, plasticizers and the insecticides through domestic, agricultural, medical and industrial activities is causing a

damaging effect to our environment by the production of various pathogens and disease causing organisms [5]. There is an urgent need to develop some method to treat the bacterial diseases as the emerging pathogens have developed resistance against most of the antibacterial and antimicrobial agents. In the recent days, the nano-sized drug carriers and the antibacterial agents have proved to be efficient against most of the pathogens and have shown a remarkable performance in the treatment of infectious diseases [6]. Currently, the NiO NPs have much fascinated the researchers for their p-type conductivity and a direct band gap of 3.6–4.0 eV along with the distinctive applications. These NPs have been extensively used for anti-microbial activity, catalysis, photocatalysis, in gas sensors, electrochemical films, smart windows and photo-electronic devices [7–11]. The non-toxicity, easy and cheap availability and photo-stability of NiO NPs make them suitable photocatalysts for the mineralization of various organic pollutants. Many researchers have manipulated NiO NPs for antibacterial activities and for the degradation of dyes [12–15]. The antibacterial activity of the NPs is dependent on the size, stability and concentration and they provide a greater retention time during the antibacterial activity while interacting with the bacteria [16]. The *B. ciliata* plant grows between 7000 and 10,000 feet in the temperate Himalayas, from Kashmir to Bhutan. Bergenin, Tannic acid, Gallic acid, Stigmesterol, -Sitosterol, Catechin, (+)-Afzelechin, 1,8-cineole, Isovalaric acid, (+)-(6S)-parasorbic acid, Arbutin, -eudesmol, 3-methyl-2-buten-1-ol, (Z)-asarone, Terpin are the phytochemicals identified in *B. ciliate* and act as bioreductants and capping agents in the production and stabilization of metals and metal oxide nanoparticles. *B. ciliate* is a medicinal plant locally used to cure a variety of illnesses (including diarrhoea and vomiting), as well as fever, cough, and lung infections [17].

Different applications of NiO NPs were reported after they were synthesized in different ways. However, they were not used for many applications after the same synthesis. Moreover, the use of NiO NPs as photocatalysts against Rh-6G, an antibacterial agent against pathogenic bacteria, and ABTS-free radical scavenging agents has yet to be reported. Here in this project, the NiO NPs have been synthesized by using a time-saving, economical, and environmentally friendly plant-mediated method, where *B. ciliata* leaf extract was used as a reducing and capping agent and nickel nitrate was used as the source of nickel. The physicochemical properties were investigated via different techniques such as XRD, SEM, TEM, EDX, FTIR and UV-Visible spectroscopy. The as-fabricated NPs were manipulated for photocatalytic, antibacterial and antioxidant studies.

2. Materials and Methods

2.1. Chemical Used

The analytical grade chemicals obtained from Sigma-Aldrich were manipulated in the current project. Nickel nitrate, ethanol, rhodamine 6G, and Agar nutrients were used in this project. All the required solutions were prepared in distilled water.

2.2. Preparation of Plant Extract

The green leaves of *B. ciliate* were collected in the month of April from Neelum valley (34.5985° N, 73.9073° E), Azad Kashmir, Pakistan. For the preparation of the aqueous extract, 20 g of *B. ciliate* leaves were boiled in 200 mL of distilled water at 70 °C. After 15 min, the aqueous extract was filtered through Whatmann No.1 filter paper to get the clear plant extract. The aqueous leaves extract was used as a reducing agent for the synthesis of nanomaterials.

2.3. Green Synthesis of NiO NPs

For the typical synthesis of NiO NPs, 5 mM stock solution was prepared in 1000 mL by dissolving 1.45 g of $Ni(NO_2)_2.6H_2O$, and 80 mL of this solution was mixed with 20 mL B ciliate. The mixture was heated and stirred for 15 min and then the pH was adjusted at 10 by the dropwise addition of NaOH solution. The heating and stirring was continued for 45 min further and the greenish gel formed was aged for 24 h and was then washed

with deionized water thrice. The solid product was oven dried at 150 °C and stored in a polyethylene bottle.

2.4. Physicochemical Characterization

The crystalline nature of the synthesized NiO NPs was studied by XRD model Philips X'Pert and the crystallite size was estimated using Debye-Scherrer equation. The microstructure and surface topology was studied with SEM Model JEOL JSM-5600LV, Tokyo, Japan and Hitachi HT7800 transmittance electron microscope (TEM) Cleveland, TN, USA. Energy-dispersive X-ray (EDX) analysis was carried out by using EDX model INCA 200, Oxford Instruments, Oxfordshire, UK coupled with SEM to confirm the composition of the sample. The UV-Visible spectroscopic analysis was carried out to study the optical properties using Shimadzu (UV-800) provided by Thermo Fisher Scientific Waltham, MA, USA whereas the surface functional moieties was investigated through FTIR model Nicolet 560, Thermo Fisher Scientific Waltham, MA, USA was operated in the range between 4000 and 400 cm^{-1} [18].

The photocatalytic efficacy of NiO NPs was evaluated during the degradation of Rh-6G in the presence solar light in month June between 11 a.m. to 3 p.m. For the typical photochemical reaction, 25 mg of the catalyst was added to the reaction vessel containing 70 mL Rh-6G solution and was stirred in the dark for half hour. Afterward, the reaction mixture was irradiated under solar light and the UV analysis was carried out after a specific time interval (i.e., 5, 10, 20, 40, 60, 80, 100, 120, 140, 160 and 180 min). The decrease in the absorbance maxima with the passage of time suggests the degradation of Rh-6G.

2.5. Antibacterial Assay

The antibacterial activity of the NiO NPs was examined against the GPB (*S. aureus* (ATCC # 6538)) and GNB (*E. coli* (ATCC # 15224)) using the Agar well diffusion method. The plates were prepared by mixing Agar nutrients in deionized water and solidified naturally at room temperature. The bacterial culture grown overnight was spread over the media and the wells were bored with a polystyrene tip. The stock suspension was prepared by ultrasonic dispersion of 5, 15, 25 and 50 mg of NiO NPs in 5 mL deionized water and 100 µL was added into each well. The plate were then incubated at 37 °C, and after 24 h, the zone of inhibition was measured in millimetres (mm) as the activity of NiO NPs.

2.6. Antioxidant Assay

Firstly, the $ABTS^{\bullet+}$ was generated by nixing 5mM potassium persulphate and 14 mM of ABTS and kept in dark for 16 h and the absorbance of the solution was checked at 734 nm. The stock suspensions of NiO NPs was prepared by ultrasonic dispersion of 5, 25, 50, 75, 100 and 200 µg in 1 mL for 30 min at room temperature. The 0.2 mL of NiO NPs suspension and 0.15 mL of $ABTS^{\bullet+}$ solution was mixed and aged for 30 min and then subjected to UV analysis to check the absorbance at 734 nm. The percentage of ABTS radical inhibition activity was determined by using Equation (1); where Ai is the absorbance of the sample and Ao is the absorbance of the control.

$$\%RSA = \left[\frac{A_o + A_i}{A_o}\right] \times 100 \quad (1)$$

3. Results and Discussion

3.1. Physicochemical Study

3.1.1. XRD Analysis

The X-ray diffractogram of NiO NPs shown in Figure 1 possesses the diffraction peaks at two theta positions, 37.20, 43.31, 63.86, 75.36 and 79.43, corresponding to miller indices of plane (001), (−111), (−311), (−221) and (−402). In all these bands the hkl values exactly matched the data listed in JCPDS card 01-072-1464, confirming the monoclinic geometry of the crystals, with space of C2/m. The length of a coordinate is 5.1150 Å whereas those b and c coordinates are equal to 2.9580 Å. The alpha and gamma are equal (90°) although

beta is equal to 125.19°. The XRD data briefly explain the NiO crystal quality, where the intense diffraction bands with narrow FWHM suggest the formation of highly crystalline material. Furthermore, that all the bands appeared is due to NiO, so no other peak seen in the diffractogram suggests the formation of a highly pure sample. The average crystallite size was found to be 27.45 nm, whereas 1.34% lattice strain was found in the crystal.

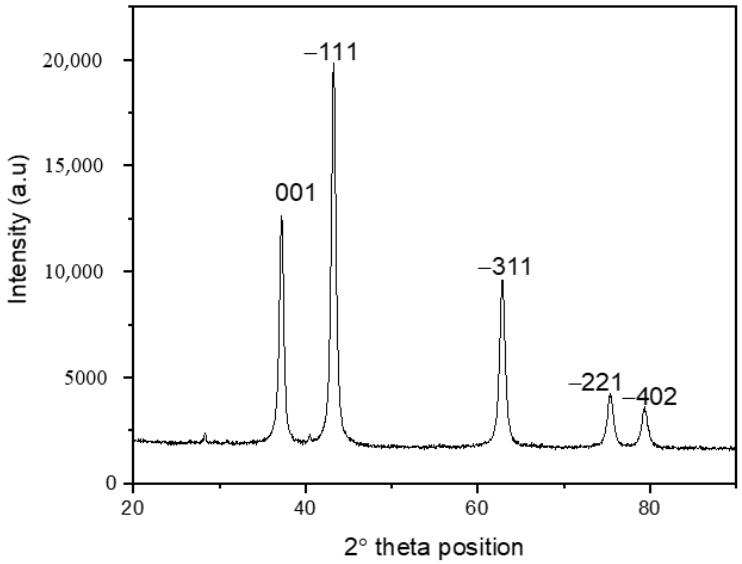

Figure 1. XRD pattern of NiO NPs.

3.1.2. Microstructure Analysis

The SEM micrograph shown in Figure 2a shows that well defined shaped particles are formed, which exhibit clear boundaries. The majority of the particles exhibited are square-shaped while other polyhedral particles are also present. The particle distributions are not smooth and several cavities are seen in the micrograph. The surface morphology of the biogenically fabricated NiO NPs was investigated through a scanning electron microscope. It is seen from the figure that the particles are highly agglomerated due to high energy and high surface area to volume ratio. The TEM analysis (Figure 2b) was carried out in the study the morphology of the synthesized NiO NPs, where most of the particles seem to be tetrahedral. Beside these, few pseudo-spherical and polyhedral particles are also observed. The particles are evenly distributed and possess well defined boundaries, whereas few particles are closely packed together. The particle sizes estimated from the TEM micrograph using ImageJ software range from 23.89 to 62.50 with an average size of 49.35 nm.

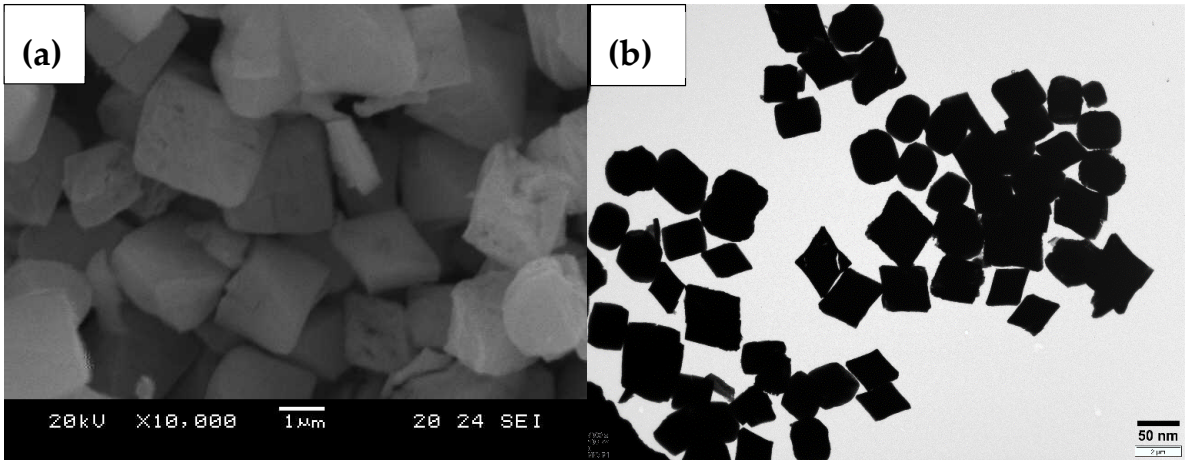

Figure 2. SEM (**a**) and TEM (**b**) micrographs of NiO NPs.

3.1.3. UV-Visible and EDX Analysis

The literature survey shows that the UV-Visible absorbance for NiO NPs was reported at 284, 310 and 381 nm, however, in the present study the absorbance edge was located at 327.62 nm (Figure 3), to which the synthesized NiO NPs showed photo-response in the UV region [10]. Several studies have been reported on NiO synthesized via both chemical and green methods, with absorbance in the range of 320–330 nm, the shift between this is due to the confinement of electron-hole carrier and responsible for the optical transition of the valence electron to conduction band, which are used to calculate the band gap energy [3,19]. The band gap energy calculated on the basis of basis of absorbance edge was 3.78 eV, which was found to be similar to that reported previously [11]. The elemental composition and purity percentage of the NiO NPs was determined through the EDX analysis and the spectrum obtained confirms the presence of Ni and O as shown as inset in Figure 3. The weight percentages of Ni and O obtained were 87.72% and 10.94%, respectively. The 0.93% C present in the sample is due to the use of carbon tape during analysis whereas the 0.41% Mn that was present in the sample is an impurity, which might be due to the use of plant leaves extract.

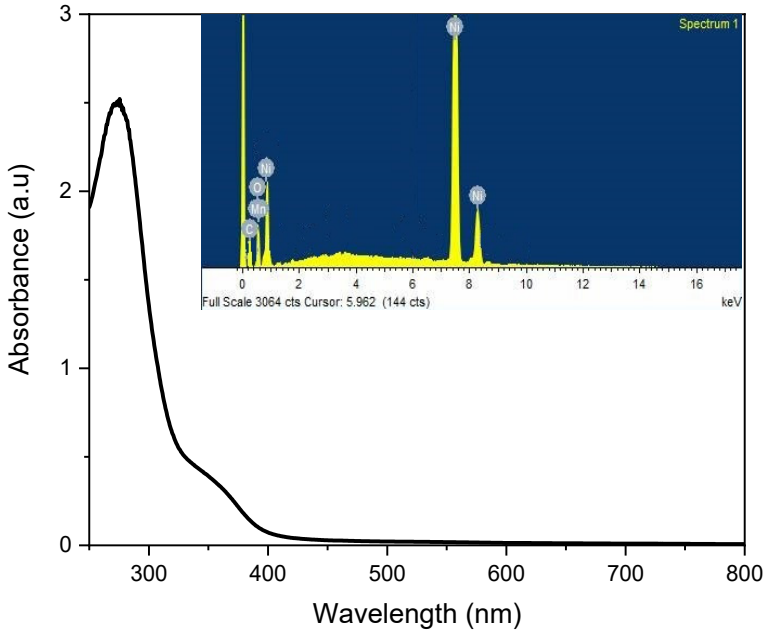

Figure 3. UV-visible spectrum (inset: EDX spectrum) of NiO NPs.

3.1.4. FTIR Analysis

The FTIR spectrum shown in Figure 4 exhibits the characteristic peaks for NiO NPs in the range of 1236 to 440 cm^{-1}, whereas the other peaks related with water molecules and phytochemicals occurred in the sample due to the use of plant leaves extract. The peaks at 440.21 and 545.23 cm^{-1} are due to the wagging and bending vibration of terminal O-H and Ni-O groups, respectively [13]. The band at 1020.52, 1110.80 and 1236.38 cm^{-1} is because of Ni-O, terminal Ni-OH and O-Ni-O stretching of the lattice structure, respectively [20]. The peaks at 1383.31 cm^{-1} are due to the nitro group, which is due to the use of nickel nitrate as a precursor to salt during synthesis [21]. The peaks at 1648.44 and 3450.06 cm^{-1} were due to the starching bending vibration of water molecules, respectively, whereas the peak at 3649.66 cm^{-1} is attributed to N-H moiety, which might be due to the utilization of plant leaves extract during synthesis [22].

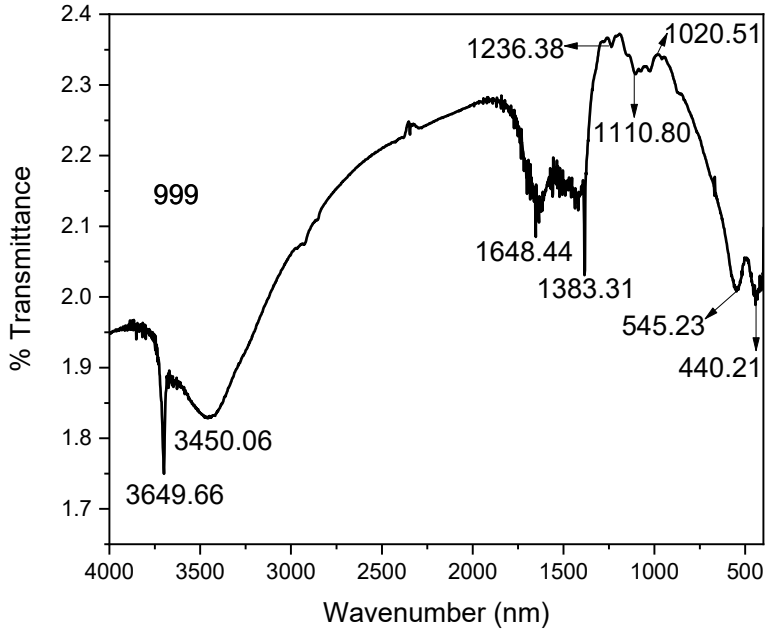

Figure 4. FTIR spectrum of NiO NPs.

3.2. Photocatalytic Activity

Figure 5 exhibits the photocatalytic degradation of the Rh-6G using plant-mediated NiO NPs. The NiO NPs were introduced to the solution at room temperature and were analysed under solar light at a wavelength of 526 nm. The decrease in absorbance maxima at the same wavelength indicates the degradation of dye molecules under solar light irradiation as shown in Figure 5a. The photocatalytic efficiency of biogenically fabricated NiO NPs was analysed under the full light spectrum for the degradation of Rh-6G. The 60 mL of the stock solution was transferred to a reaction vessel and 10 mg of the catalyst was introduced to the vessel. To establish the adsorption-desorption equilibrium, the solution was first stirred in the dark for almost 30 min. Figure 5b [23]. After stirring in the dark for 30 min the liquid samples were analysed spectrophotometrically after definite intervals of time (5, 10, 20, 40, 60, 80, 100,120, 140, 160, 180 min) and bright colour faded with the passage of time. The decrease in absorbance maxima was noted at 526 cm^{-1} and other less intense peaks as a function of time interval as shown in Figure 5b, which shows that the degradation of Rh-6G was gradual with passage of time. The sharp increase in the degradation process was seen up to 20 min, where a comparatively steady increase in the degradation was experienced above 20 min. The slow increase in the degradation might be due to a minute dye adsorption on the catalyst surface, reducing the exposure of the catalyst to solar light. Equations (2) and (3) were used to calculate the percentage degradation and degradation rate constant of the photocatalytic reaction. The after 180 min percentage degradation of Rh-6G was found to be 92.17% with a degradation rate of 2.402×10^{-2}/min (Figure 5c,d) [24].

$$\% \, Degradation = \frac{C_o \times C_i}{C_o} \times 100 \tag{2}$$

$$ln\left(\frac{C}{C_o}\right) = -kt \tag{3}$$

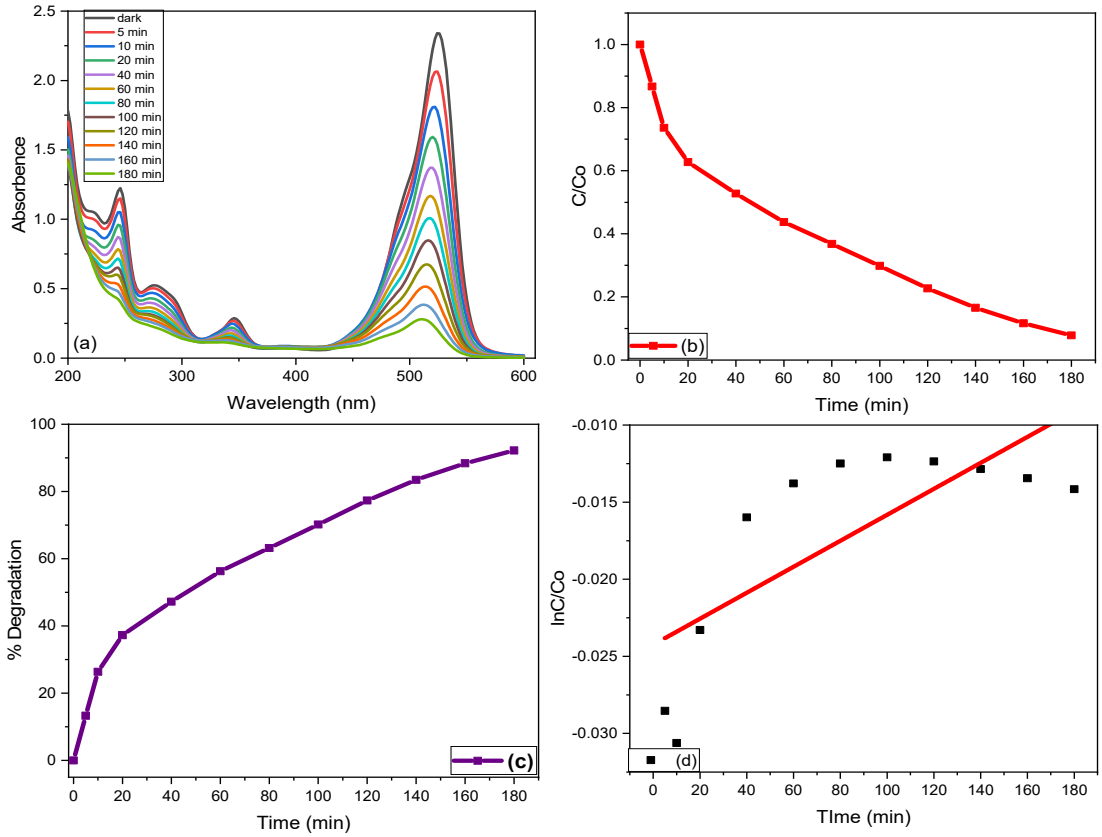

Figure 5. (**a**) Degradation profile; (**b**) C/C_o plot; (**c**) % degradation; (**d**) Degradation rate constant of Rh-6G in the presence of NiO NPs.

3.3. Antibacterial Activity

The antibacterial efficacy of the NiO NPs was tested against *E. coli* (ATCC # 15224) and *S. aureus* (ATCC # 6538) and the inhibition zones were measured in millimetres (Table 1), which shows that the activity gradually increases with increasing concentration of NiO suspension in the wells (Figure 6a,b). The minimum inhibition concentration for E. coli and S. aureus under the experimental condition was 5 mg/5 mL and 25 mg/5 mL respectively. A similar finding was also reported previously, suggesting that larger numbers of NiO NPs in the suspension are able to produce more Ni^{2+} ions results into the extensive penetration inside the bacterial cell [25]. The antibacterial activity of NiO NPs at a higher concentration (50 mg/5 mL) was almost comparable with standard drugs. The activity results also depict that the inhibition zone was larger in the case of GNB as compared to GPB, which might be due to the difference in the cell wall composition and surface charges. The cell wall of GPB consists of multiple peptidoglycans layers, whereas the GNB has few peptidoglycans layers in the cell wall. The former provide more strength to GPB cell as compared to GNB cell and prevent/control the penetration of Ni^{2+} ions [26]. The Ni^{2+} ions not only accumulate on the surface but also penetrate the bacterial cell, disturbing the cytoplasmic activity. It has been suggested that the respiration process was greatly inhibited due to the interaction of Ni^{2+} with the thiol group of the proteins molecule, which eventually led to the death of bacteria [27]. This concept attributes NiO NPs toxicity to the solubility of Ni^{2+} in the media, which includes microorganisms. The disintegration phenomena is rather debatable, despite the fact that it has been adopted and accepted. However, it was assumed that the Ni^{2+} release mechanism is controlled by the physicochemical characteristics of the particles, which include porosity, concentration, particle size, and morphology and media chemistry like pH, UV light, exposure duration and the presence of additional components. However, the impact of these factors is not well understood [28].

Table 1. Antibaterial activity of NiO NPs against *E. coli* and *S. aureus* at different concentration.

Bacteria	Zones of Inhibition Measured in Millimeter (mm) with Error of ±2					
	5 mg/5 mL	15 mg/5 mL	25 mg/5 mL	50 mg/5 mL	PC	Solvent
E. coli	1.87	3.93	8.63	13.09	14.72	00
S. aureus	00	00	4.01	10.29	12.37	00

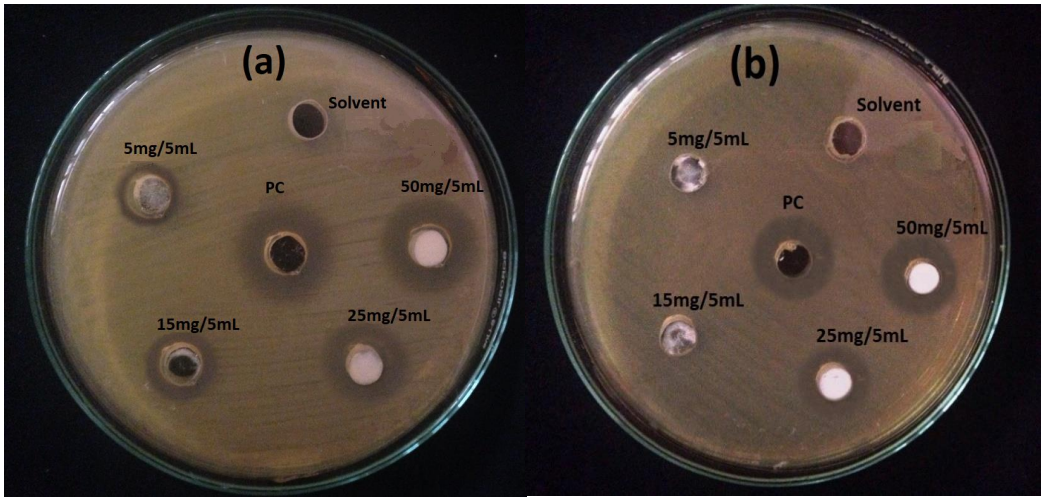

Figure 6. Pictographic illustration of antibacterial activity of NiO NPs against *E. coli* (**a**) and *S. aureus* (**b**).

3.4. Antioxidant Activity

The antioxidant activity of NiO NPs was screened against the $ABTS^{\bullet+}$ in methanolic solution and the activity was compared with ascorbic acid used as control and results obtained was illustrated in Figure 7. The different concentration of NiO NPs and ascorbic acid was treated with a solution containing $ABTS^{\bullet+}$ to determine the percentage radical scavenging activity [29]. It was observed that the antioxidant activity increased with increasing concentration of the both the samples, suggest that a larger number of antioxidants is required to neutralize the $ABTS^{\bullet+}$ radical cation. The IC_{50} (μgmL^{-1}) value is the concentration of antioxidant that can neutralize 50% of the $ABTS^{\bullet+}$ radical cation. The calculated IC_{50} value for NiO NPs is 49.63 μgmL^{-1} and that for ascorbic acid is 14.99 μgmL^{-1}, suggesting that the activity of NiO NPs was less than ascorbic acid.

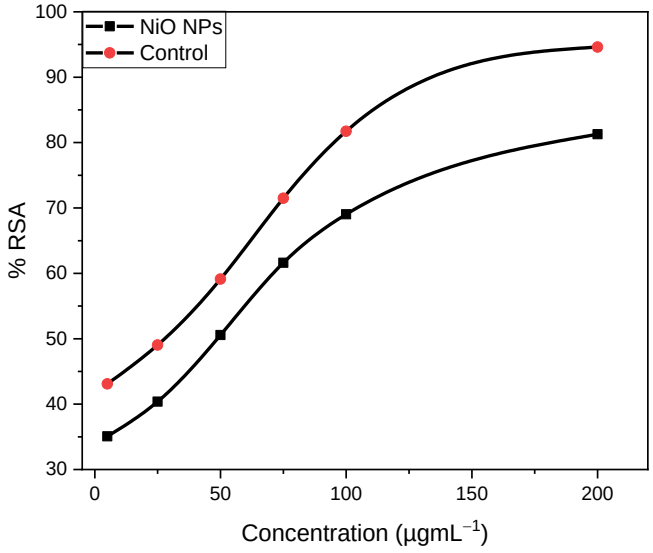

Figure 7. Percentage radical scavenging activity of NiO NPs and control (ascrobic acid).

4. Conclusions

An eco-friendly and efficient process was followed for the synthesis of highly crystalline nano-sized NiO NPs, which exhibit enhanced photocatalytic, antibacterial and antioxidant potential. The examined physicochemical properties confirm the formation of extremely pure NiO NPs, where the majority of the particles exhibit tetrahedral geometry. The photocatalytic results suggest that Rh-6G was efficiently degraded in the presence of NiO NPs. The higher antibacterial activity against *E. coli* as compared to *S. aureus* might be due to the difference in the cellular structure. The photocatalytic, antibacterial and antioxidant activities suggest that the synthesized NiO NPs is a multifunction candidate and must be utilized in future for the purification of waste water, inhibition of bacterial growth and scavenging of free radicals. This study provides sensible results that prove that NiO NPs are a multifunctional material that can be obtained by a very simple method and can be utilized for other applications in future.

Author Contributions: Conceptualization, R.M. and S.H.; methodology, R.M. and S.H.; validation, R.M., S.H. and F.U.R.; formal analysis, F.U.R.; investigation, S.H. and F.U.R.; resources, R.M. and S.H.; data curation, S.H., A.H. and F.U.R.; writing—original draft preparation, S.H., R.E. and F.U.R.; writing—review and editing, R.M., M.B.A., A.M. and S.H.; visualization, S.U.D.; supervision, R.M. and S.H.; project administration, R.M. and S.H.; funding acquisition, M.B.A., A.M. and A.H. All authors have read and agreed to the published version of the manuscript.

Funding: This research received no external funding.

Data Availability Statement: Not applicable.

Acknowledgments: The authors are grateful to the Deanship of Scientific Research for funding this article by Taif University Researchers Supporting Project number (TURSP-2020/28), Taif University, Taif, Saudi Arabia.

Conflicts of Interest: The authors declare no conflict of interest.

References

1. Barzinjy, A.A.; Hamad, S.M.; Aydın, S.; Ahmed, M.H.; Hussain, F.H.S. Green and eco-friendly synthesis of Nickel oxide nanoparticles and its photocatalytic activity for methyl orange degradation. *J. Mater. Sci. Mater. Electron.* **2020**, *31*, 11303–11316. [CrossRef]
2. Br, S.; Xr, J. Effect of calcination time on structural, optical and antimicrobial properties of nickel oxide nanoparticles. *Theor. Comput. Sci.* **2016**, *3*, 149–159. [CrossRef]
3. El-Kemary, M.; Nagy, N.; El-Mehasseb, I. Nickel oxide nanoparticles: Synthesis and spectral studies of interactions with glucose. *Mater. Sci. Semicond. Process.* **2013**, *16*, 1747–1752. [CrossRef]
4. Suresh, K.C.; Balamurugan, A. Evaluation of structural, optical, and morphological properties of nickel oxide nanoparticles for multi-functional applications. *Inorg. Nano-Metal. Chem.* **2020**, *51*, 296–301. [CrossRef]
5. Lingaraju, K.; Raja Naika, H.; Nagabhushana, H.; Jayanna, K.; Devaraja, S.; Nagaraju, G. Biosynthesis of nickel oxide nanoparticles from euphorbia heterophylla (L.) and their biological application. *Arab. J. Chem.* **2020**, *13*, 4712–4719. [CrossRef]
6. Ezhilarasi, A.A.; Vijaya, J.J.; Kaviyarasu, K.; Zhang, X.; Kennedy, L.J. Green synthesis of nickel oxide nanoparticles using solanum trilobatum extract for cytotoxicity, antibacterial and photocatalytic studies. *Surf. Interfaces* **2020**, *20*, 100553. [CrossRef]
7. Feiona, T.A.; Sabeena, G.; Bagavathy, M.S.; Pushpalaksmi, E.; Samraj, J.J. Recent advances in the synthesis and characterization of nanoparticles: A green adeptness for photocatalytic and antibacterial activity. *Nat. Environ. Pollut. Technol.* **2021**, *20*, 657–663. [CrossRef]
8. Mokoena, T.P.; Swart, H.C.; Motaung, D.E. A review on recent progress of p-type nickel oxide based gas sensors: Future perspectives. *J. Alloys Compd.* **2019**, *805*, 267–294. [CrossRef]
9. Arora, A.K.; Jaswal, V.S.; Singh, K.; Singh, R. Applications of metal/mixed metal oxides as photocatalyst: A review. *Orient. J. Chem.* **2016**, *32*, 2035–2042. [CrossRef]
10. Niklasson, G.A.; Granqvist, C.G. Electrochromics for smart windows: Thin films of tungsten oxide and nickel oxide, and devices based on these. *J. Mater. Chem.* **2007**, *17*, 127–156. [CrossRef]
11. Danjumma, S.G.; Abubakar, Y.; Suleiman, S. Nickel Oxide (NiO) devices and applications: A review. *Int. J. Eng. Res. Technol.* **2019**, *V8*, 461–467. [CrossRef]
12. Hameed, A.; Gombac, V.; Montini, T.; Graziani, M.; Fornasiero, P. Synthesis, Characterization and photocatalytic activity of NiO–Bi_2O_3 nanocomposites. *Chem. Phys. Lett.* **2009**, *472*, 212–216. [CrossRef]

13. Haq, S.; Dildar, S.; Ali, M.B.; Mezni, A.; Hedfi, A.; Shahzad, M.I.; Shahzad, N.; Shah, A. Antimicrobial and antioxidant properties of biosynthesized of NiO nanoparticles using raphanus sativus (R. sativus) extract. *Mater. Res. Express* **2021**, *8*, 055006. [CrossRef]
14. Sone, B.T.; Fuku, X.G.; Maaza, M. Physical & electrochemical properties of green synthesized bunsenite NiO nanoparticles via callistemon viminalis' extracts. *Int. J. Electrochem. Sci.* **2016**, *11*, 8204–8220. [CrossRef]
15. Angel Ezhilarasi, A.; Judith Vijaya, J.; Kaviyarasu, K.; John Kennedy, L.; Ramalingam, R.J.; Al-Lohedan, H.A. Green synthesis of NiO nanoparticles using aegle marmelos leaf extract for the evaluation of in-vitro cytotoxicity, antibacterial and photocatalytic properties. *J. Photochem. Photobiol. B Biol.* **2018**, *180*, 39–50. [CrossRef]
16. Anand, G.T.; Nithiyavathi, R.; Ramesh, R.; John Sundaram, S.; Kaviyarasu, K. Structural and optical properties of nickel oxide nanoparticles: Investigation of antimicrobial applications. *Surf. Interfaces* **2020**, *18*, 100460. [CrossRef]
17. Sinha, S.; Murugesan, T.; Maiti, K.; Gayen, J.R.; Pal, M.; Saha, B.P. Evaluation of anti-inflammatory potential of bergenia ciliata sternb. rhizome extract in rats. *J. Pharm. Pharmacol.* **2010**, *53*, 193–196. [CrossRef]
18. Hamid, A.; Haq, S.; Ur Rehman, S.; Akhter, K.; Rehman, W.; Waseem, M.; Ud Din, S.U.; Zain-ul-Abdin; Hafeez, M.; Khan, A.; et al. Calcination temperature-driven antibacterial and antioxidant activities of fumaria indica mediated copper oxide nanoparticles: Characterization. *Chem. Pap.* **2021**, *75*, 4189–4198. [CrossRef]
19. Sagadevan, S.; Podder, J. Investigations on structural, optical, morphological and electrical properties of nickel oxide nanoparticles. *Int. J. Nanoparticles* **2015**, *8*, 289–301. [CrossRef]
20. Goel, R.; Jha, R.; Ravikant, C. Investigating the structural, electrochemical, and optical properties of p-type spherical nickel oxide (NiO) nanoparticles. *J. Phys. Chem. Solids* **2020**, *144*, 109488. [CrossRef]
21. Shah, A.; Haq, S.; Rehman, W.; Muhammad, W.; Shoukat, S.; Rehman, M. Photocatalytic and antibacterial activities of paeonia emodi mediated silver oxide nanoparticles. *Mater. Res. Express* **2019**, *6*, 045045. [CrossRef]
22. Ahmad, S.; Fahmina, B.; Aftab, Z.; Mondal, H.; Kareem, A.; Ullah, A. Photocatalytic degradation of carcinogenic congo red dye in aqueous solution, antioxidant activity and bactericidal effect of NiO nanoparticles. *J. Iran. Chem. Soc.* **2020**, *17*, 215–227. [CrossRef]
23. Shoukat, S.; Rehman, W.; Haq, S.; Waseem, M.; Shah, A. Synthesis and characterization of zinc stannate nanostructures for the adsorption of chromium (VI) ions and photo-degradation of rhodamine 6G. *Mater. Res. Express* **2019**, *6*, 115052. [CrossRef]
24. Haq, S.; Rehman, W.; Waseem, M.; Meynen, V.; Awan, S.U.; Khan, A.R.; Hussain, S.; Zain-ul-Abdin; Din, S.U.; Hafeez, M.; et al. Effect of annealing temperature on structural phase transformations and band gap reduction for photocatalytic activity of mesopores TiO_2 nanocatalysts. *J. Inorg. Organomet. Polym. Mater.* **2021**, *31*, 1312–1322. [CrossRef]
25. Haq, S.; Yasin, K.A.; Rehman, W.; Waseem, M.; Ahmed, M.N.; Shahzad, M.I.; Shahzad, N.; Shah, A.; Rehman, M.U.; Khan, B. Green synthesis of silver oxide nanostructures and investigation of their synergistic effect with moxifloxacin against selected microorganisms. *J. Inorg. Organomet. Polym. Mater.* **2020**, *31*, 1134–1142. [CrossRef]
26. Haq, S.; Ahmad, P.; Khandaker, M.U.; Faruque, M.R.I.; Rehman, W.; Waseem, M.; Din, S.U. Antibacterial, antioxidant and physicochemical investigations of tin dioxide nanoparticles synthesized via microemulsion method. *Mater. Res. Express* **2021**, *8*, 035013. [CrossRef]
27. Shah, A.; Tauseef, I.; Ali, M.B.; Yameen, M.A.; Mezni, A.; Hedfi, A.; Haleem, S.K.; Haq, S. In-vitro and in-vivo tolerance and therapeutic investigations of phyto-fabricated iron oxide nanoparticles against selected pathogens. *Toxics* **2021**, *9*, 105. [CrossRef] [PubMed]
28. Sirelkhatim, A.; Mahmud, S.; Seeni, A.; Kaus, N.H.M.; Ann, L.C.; Bakhori, S.K.M.; Hasan, H.; Mohamad, D. Review on zinc oxide nanoparticles: Antibacterial activity and toxicity mechanism. *Nano-Micro Lett.* **2015**, *7*, 219–242. [CrossRef]
29. Haq, S.; Abbasi, F.; Ben Ali, M.; Hedfi, A.; Mezni, A.; Rehman, W.; Waseem, M.; Khan, A.R.; Shaheen, H. Green synthesis of cobalt oxide nanoparticles and the effect of annealing temperature on their physiochemical and biological properties. *Mater. Res. Express* **2021**, *8*, 075009. [CrossRef]